2024년 2월

박사학위 논문

Characterization of spontaneous osteopetrosis models on RANKL-dysfunctional mice

조 선 대 학 교 대 학 원

의 과 학 과

주 지 웅

Characterization of spontaneous osteopetrosis models on RANKL-dysfunctional mice

RANKL 비활성화 마우스의 골경화증 질환 모델 연구

2024년 2월 23일

조 선 대 학 교 대 학 원

의 과 학 과

주 지 웅

Characterization of spontaneous osteopetrosis models on RANKL-dysfunctional mice

지도교수 임 원 봉

이 논문을 약학 박사학위신청 논문으로 제출함

2023년 10월

조 선 대 학 교 대 학 원

의 과 학 과

주 지 웅

주지웅의 박사학위 논문을 인준함

위원장 손 홍 문 (인)

위 원 김 동 휘 (인)

위 원 이 광 철 (인)

위 원 현 훈 (인)

위 원 임 원 봉 (인)

2024년 1월

조 선 대 학 교 대 학 원

CONTENTS

LIST OF FIGURES

ABSTRACT

RANKL 비활성화 마우스의 골경화증 질환 모델 연구

주 지 웅

지도교수 : 임 원 봉

조선대학교 대학원 의과학과

목적: RANKL(핵 인자-κB 리간드의 수용체 활성화제)로도 알려진 종양 괴사 인자 슈퍼패밀리 멤버 11 (TNFSF11)은 파골세포 세포막에 존재하는 RANK에 결합하는 핵심 파골세포 자극 인자이다. 돌연변이 마우스 모델은 관련 질병의 유전적 메커니즘을 평가하는 강력한 도구로서 본 연구에서는 마우스에서 Tnfsf11의 이형접합성 유전적 돌연변이가 뼈 재형성 및 메커니즘을 이해하는 데 유용하다는 것을 보고하고자 하였다. 2011년 Jackson Laboratory에서 발견된 Tnfsf11gum 마우스는 골수 조직에서 RANKL의 비활성화와 관련된 유전적 변화를 이해하는 데 사용되었다.

대상 및 방법: 이에 본 연구에서는 $Tnfsf11^{gum/+}$ 및 $Tnfsf11^{+/+}$ 마우스에서 Micro-CT 관찰, ELISA 분석, 조직학적 평가 및 mRNA(RNA-Seq)의 대규모 병렬 시퀀싱을 통해 비교 분석을 수행하였다

결과: $Tnfsf11^{gum/+}$ 마우스는 $Tnfsf11^{+/+}$ 마우스와 비교하여 골수에서 심각한 골석화성 골수강과 상당히 낮은 혈청 RANKL 수준뿐 만 아니라 낮은 TRAP 양성 파골세포 수를 보여주었다. 그럼에도 불구하고, $Tnfsf11^{gum/+}$ 및 $Tnfsf11^{+/+}$ 마우스 사이에는 치아 맹출과 혈청 OPG의 변화가 감지되지 않았다. 또한, 조골세포 증식 및 분

화에 관여하는 유전자 중 Gli1, Slc35b2, Lrrc17 및 Junb의 발현 증가와 파골세포의 증식 및 분화에 관여하는 유전자 중 Tclirg1, Junb, Anxa2 및 Atp6ap1 유전자의 발현 증가가 관찰되었다.

결론: 본 연구는 Tnfsf11의 단일 유전자 돌연변이가 골수강에서 조골세포 및 파골세포의 활성과 관련된 유전자의 큰 변화 없이도, 뼈 재흡수 불안정성을 초래한다는 것을 보여주며 골 생물학 연구에서 골 흡수 실험 동물 모델로서 중요한 자원을 제공할 수 있는 것을 보여주었다.

색인단어: RANKL mutant type, OPG, LGR4, 파골세포, 골다공증

I. INTRODUCTION

The receptor activated NF-kappa B ligand (RANKL), also known as Tnfsf11, OPGL (osteoprotegerin ligand), ODF (osteoclast differentiation factor), and TRANCE (tumor necrosis factor-related activation-induced cytokine), is a cytokine in the TNF superfamily.[1]. It is a substance that regulates the differentiation and proliferation of osteoclasts. Tnfsf11 is expressed on osteoblasts or T cells and then, it binds to TNFRSF11B/OPG and to TNFRSF11A/RANK on osteoclasts and precursor cells [2]. In particular, the binding of TNFRSF11A/RANK is known to trigger osteoclast differentiation and bone-resorbing activities, as well as the maintenance of mature osteoclast activation [3]. In humans, the Tnfsf11 gene is located on chromosome 13 (13q14.11) and encodes a glycoprotein called RANKL, which consists of 317 amino acids [4]. RANKL is a type II transmembrane protein with an extracellular domain at the carboxy terminus. It shares 85% identity in amino acid sequence between humans and mice [5]. The ectodomain of RANKL is cleaved by enzymes such as matrix metalloproteinases and released into the bloodstream and extracellular environment as a soluble form [6]. RANKL released in soluble form from active osteoblasts is the only ligand that binds to the extracellular domain of RANK. The binding of RANKL to RANK forms a trimer and activates signaling pathways, leading to the differentiation of pre-osteoclasts and the activation of the mature form [7]. Therefore, it is crucial to characterize and identify the genes expressed in association with Tnfsf11 in order to understand the genetic basis of the bone remodeling process.

To investigate various genetic functions, the experimental mouse model is used to establish various disease models. The skeletal structures of each mouse are remarkably similar to the homologous bones in humans, and the genes associated with bone remodeling are shared between the two species [8]. The recent understanding of bone physiology in mice has been advanced by the use of reverse genetic tools and resources available for mice [9,10], such as knockout alleles, cre driver and loxP-flanked target genes, and now genome editing platforms that enable rapid modification of specific alleles [11]. While incredibly informative and productive, hypothesis-driven approaches are inevitably biased by preliminary data associated with a given gene or pathway [12]. Genomic or phenotype-based screens provide an unbiased method for identifying new genes and their functions that underlie a specific phenotype or condition [13]. Spontaneous mutations provide an additional level of unbiased discovery, as new variations can emerge on any genetic background, revealing a phenotype that might have been overlooked on a limited number of inbred backgrounds [14]. These advances could improve the ability to identify numerous new spontaneous models of bone disorders, contributing to a better understanding of the function of genes and their pathways that play a pivotal role in bone development.

Here, we present the Tnfsf11 mutant resource, which is the result of a long-standing effort to capitalize on the large mouse breeding colonies at the Jackson Laboratory. The scale of these colonies has led to the emergence of heterozygous spontaneous mutants, providing mouse models of bone dysmorphology. The aim of the present study is to determine whether the potential regulatory sequences

near the murine Tnfsf11 gene are involved in its expression, and consequently, in bone metabolism and tooth eruption. These mutant models include genes for which all existing models are lethal, novel genes not previously associated with bone development, and genes where the specific genetic background reveals a disease model that is masked by typically used inbred strains. The mice are available from the resource, and our ongoing screening process routinely identifies new models that will contribute to the collection. Together, this resource provides a unique and rich source of tools for discovering bone biology.

II. MATERIALS AND METHODS

Animals and husbandry

The spontaneous mutant mouse (Tnfsf11$^{gum/+}$) was discovered in 2011 at Jackson Laboratory (JAX; Bar Harbor, ME) in a large-scale production colony of BALB/cJ mice. These procedures were presented by The Jackson Laboratory's Institutional Animal Care and described in previous study [8]. These F2 mice were transferred to the Animal Facility of Chosun University in Korea where they were maintained in a climate-controlled environment. Tnfsf11 wild type mice as well as heterozygous and homozygous Tnfsf11 mutant mice were generated from heterozygous mating. Mice were maintained either on standard laboratory diet. Mouse handling and care were followed according to Chosun University. (CIACUC2023-A0009)

Genotyping

Genomic DNA was isolated and extracted in tail clips from mice using DNase Blood & Tissue kit (Qiagen Inc., Valencia, CA), according to the manufacture's protocol. Three primers were designed for amplification of the wild-type, mutant, or both alleles in the same reaction as manufacture's provide. The primers were the following: Mutant p1 Forward 5′-ACT GGC CGA AGA ATG AAA GA-3′, Wild p2 Forward 5′-CAA GGA CCT GGG CTA TGA AC A-3′, Common p3 Forward 5′- GGG GTG TGT AAA GGG ATG TG A-3′. The primer pair p1/p3 produced a 480 bp mutant type allele, while primers p2/p3 resulted in a 342 bp wild type allele.

Body weight and survival rate measurement

To investigate the effect of Tnfsf11 gene mutations on body growth and survival,

whole body size of Tnfsf11$^{+/+}$, Tnfsf11$^{gum/gum}$ and Tnfsf11$^{gum/+}$ mice and mice survival were observed at 3weeks postnatal. Also, body weight and survival rate in ten mice of each groups were measured and monitored at each time point.

Micro-CT imaging and data acquisition

To study the formation of mineralized tissues in Tnfsf11 mutation mice, Micro-CT scanning was performed on the distal femur and maxillofacial bone tissues using a Quantum GX micro-CT imaging system (PerkinElmer, Hopkinton, MA, USA) at the Korea Basic Science Institute (KBSI) in Gwangju, Korea. The distal femur was scanned starting at the level of the growth plate, and the maxillofacial area was scanned at the maxillary level. The X-ray source was set to 90 kV and 88 mA, with a field of view of 10 mm (voxel size, 20 μm; scanning time, 4 min). The 3D imaging was displayed using 3D Viewer, a pre-existing software in the Quantum GX. Resolution was set at 4.5 μm, and images were obtained. Following the scan, the structural parameters of trabecular bone were analyzed using Analyze 12.0 software (AnalyzeDirect, Overland Park, KS, USA). Mineral femur density was estimated using a hydroxyapatite (HA) phantom (QRM-Micro CT-HA, Quality Assurance in Radiology and Medicine GmbH, Germany) and scanned using the same parameters. Bone mineral density (BMD), bone volume (expressed as a percentage of tissue volume), bone volume of bone surface (BV/BS), and trabecular number (Tb. N.) in trabecular bone and cortical area (Ct. Ar), as well as cortical thickness (Ct. Th.) in cortical bone of the femur was calculated using the ROI tool.

Analysis of serum sRANKL, OPG, and CTX

Mice was euthanized with CO_2 at a displacement rate of 50%/min and blood was collected via cardiac puncture and serum was separated from whole blood by centrifugation. The CTX-1, RANKL and OPG serum levels were determined by commercial ELISA kit (R&D Systems, MN, USA). Sample absorbance was measured at 450nm on a microplate reader (BioTek). This reading was then subtracted from absorbance recorded at 570 nm.

Histological analysis of mouse tissues

Mouse femur including skeletal tissues were collected and fixed in cold 4% formalin. And then, bone tissue was decalcified using an EDTA (0.5 M) solution before processing onto the slide glass. The decalcified bones were cut at the midpoint and embedded in paraffin blocks. The tissues were then stained with hematoxylin & eosin (H&E) or TRAP and images were acquired using an ECLIPSE Ts2R inverted microscope (Nikon, Tokyo, Japan).

Endosteal Cell Isolation

Each mice femur was extracted immediately after euthanasia. The distal and proximal epiphyses of femurs were cut away and bones were centrifuged at 13,000 rpm for 1 minute at room temperature to remove bone marrow. Periosteum was aseptically removed with a scalpel and the bone was bisected lengthwise to expose the endosteum. Femora from each mouse were combined and incubated with 4 ml of collagenase solution (3 mg/ml Collagenase Type IV in PBS, Worthington Biochemical Corp., Lakewood, NJ) inside a 5% CO_2 chamber at 37°C for 15 min under continuous agitation. Cells recovered from this initial digestion were discarded since they contained a large fraction of red blood cells. The long bones

were digested in two additional 4 ml collagenase solutions for 30 minutes each, and the cells recovered with each digestion were mixed with an equal volume of α-MEM (w/10% FBS + 1% anti-mycotic) and combined. After pelleting the cells at 2,000 x g for 5 minutes, the pellet was resuspended in 0.7 ml of PBS (w/ 0.04% BSA) and then used to prepare scRNA-seq libraries.

RNA Preparation and Quality Check

RNA was prepared from the samples with TRIzol reagent (750 μL per sample; Life Technologies, Grand Island, NY, USA) and a RNeasy mini kit (QIAGEN Inc., Valencia, CA, USA). Chloroform (150 μL) was added to the well, and the plate was then vortexed extensively. The plate was incubated at room temperature for 2-3 min and then centrifuged at 12,000 ×g for 1 min. The supernatant (350 μL) was mixed with an equal volume of 70% ethanol in a new well. Then, the RNA was extracted with the RNeasy mini Kit according to the manufacturer's instructions. RNA integrity was measured with an Agilent 2100 Bioanalyzer (Agilent Technologies, Santa Clara, CA, USA), and a sample with an RNA Integrity Number greater than or equal to 8 was considered acceptable.

Library Preparation and massively-parallel sequencing of mRNA

cDNA libraries were generated from isolated total RNA samples using TruSeq Stranded Total RNA kit with Ribo-Zero Globin (Illumina, California, United States) by following manufacturer's protocol. Quality-passed libraries were sequenced on NovaSeq6000 system (Illumina) using 100 bp paired-end protocol.

Data Processing and Differential Gene Expression Analyses

Data were analyzed and illustrated using multiple bioinformatics software under

default settings unless otherwise stated. Reads were quality-trimmed using Cutadapt1 (version 1.9. dev2) and those with low quality and short reads (<35 bp) were trimmed along with Illumina TruSeq RNA kit adapters. Reads were aligned to the reference genome (Mus Musculus GRmc38) using STAR2 (version 2.5.2b) specifying paired-end reads. Reads were assigned to features of type 'exon' in the input annotation grouped by gene_id in the reference genome using feature Counts3 (version 1.5.1). The raw counts table was filtered to remove genes consisting predominantly of near-zero counts, filtering on counts per million (CPM) to avoid artefacts due to library depth. Overall, four biological replicate datasets were generated. Abundance data were successively subjected to differential gene expression analyses. Z-scores were calculated from CPM values as described previously (Malone et al., 2011) and heatmaps generated using GraphPad Prism software (GraphPad Software).

Differential gene expression analyses and gene ontology (GO) clustering analyses were performed using Integrated Differential Expression and Pathway (iDEP.92, South Dakota State University, United States) online tool. Raw CPM values were uploaded and computed (min. CPM = 1) to identify and generate various illustrations for gene clustering and differentially expressed genes. Differential expression analysis was performed using the DEseq2 method (Love et al., 2014). PCA and Volcano plots were generated with Log2-fold change (FC) > 2 and false discovery rate (FDR) cutoff <0.05. K-Means clustering were used for performing gene enrichment analyses using GO biological processes pathway database (Ashburner et al., 2000).

Statistical analysis

All quantitative results are presented as means ± SD. Statistical significance between two groups was determined using two-tailed student's t-tests with Bonferroni multiple-comparisons test. All reported P-values were two-sided, and $P < 0.05$ were considered statistically significant. All statistical analyses were carried out using GraphPad Prism Version 7 (GraphPad Software Inc.).

III. RESULTS

Tnfsf11$^{+/+}$, Tnfsf11$^{gum/+}$ and Tnfsf11$^{gum/gum}$ mice genotype and monitoring results

All variant and wild type genotypes that were conclusively identified were identical to the genotypes identified by standard sequencing. Tnfsf11$^{+/+}$ and Tnfsf11$^{gum/gum}$ mice exhibited a single band of 342 bp and 480 bp, respectively, while Tnfsf11$^{gum/+}$ showed a double band of 342 bp and 480 bp (Fig. 1A).

At 3 weeks after birth, Tnfsf11gum/gum mice showed obvious smaller size compared to Tnfsf11$^{+/+}$ or Tnfsf11$^{gum/+}$ mice (Fig. 1B). At 1 week, there was no significant difference in body weight between Tnfsf11$^{+/+}$, Tnfsf11$^{gum/+}$, and Tnfsf11$^{gum/gum}$ mice (Fig. 1C). However, at 3 weeks, the body weight of Tnfsf11$^{gum/gum}$ mice was significantly lower than that of the other two genotypes. The survival rate of mice measured from 3 weeks after birth was also significantly lower in Tnfsf11$^{gum/gum}$ mice compared to the other two mouse species (Fig. 1D). Therefore, in the next experiment, the functionality of the Tnfsf11 gene was studied by comparing Tnfsf11$^{+/+}$ and Tnfsf11$^{gum/+}$ mice.

Radiographic results of Tnfsf11$^{+/+}$, Tnfsf11$^{gum/+}$ mice.

To investigate the function of Tnfsf11 in the mineralization of mouse bone tissue, radiographic analysis was performed using micro-CT on the femur and maxillofacial bones of mice. In Tnfsf11$^{gum/+}$ mice, compared with Tnfsf11$^{+/+}$ mice, the structure of the femur trabecular bone was significantly denser, and excessive mineralized tissue was observed (Fig. 2A). In the trabecular bone area, BMD, BV, BS/BV, and Tb. N. were significantly higher in Tnfsf11$^{gum/+}$ mice than in Tnfsf11$^{+/+}$

mice (Fig. 2B). Ct. Ar. and Ct. Th. The levels were also significantly higher in Tnfsf11$^{gum/+}$ mice in the cortical area (Fig. 2C). In the maxillofacial bone tissue of Tnfsf11$^{gum/+}$ mice, mineralized tissue was noticeably observed, but no abnormal tooth eruption was detected in either the maxillary bone or mandible (Fig. 2D).

In summary, the Tnfsf11 mutation inhibited normal bone resorption in heterozygous mice and increased abnormal mineralized tissue, but no difference was observed in tooth eruption based on the normal function of Tnfsf11.

Bone resorption marker and histologic analysis in Tnfsf11$^{+/+}$ and Tnfsf11$^{gum/+}$ mice.

To evaluate bone remodeling markers in Tnfsf11 mutation mice, CTX-1, sRANKL, and OPG levels were measured in the serum of Tnfsf11$^{+/+}$ and Tnfsf11$^{gum/+}$ mice (Fig. 3A). The Circulating CTX-1 and sRANKL levels were significantly higher in Tnfsf11gum/+ mice. However, interestingly, there was no significant difference in OPG levels between Tnfsf11$^{+/+}$ and Tnfsf11 $^{gum/+}$ mice.

In a histological assay using H&E staining, we observed that the trabecular bone was very thick, with an abnormally compacted network structure in Tnfsf11$^{gum/+}$ (Fig. 3B). However, the trabecular bone from Tnfsf11$^{+/+}$ mice femurs exhibited a normal arrangement pattern and a thick, dense network with minimal spaces. Some of the interstitial spaces between cells of trabecular bones expanded in size. Next, the histological sections of femurs were examined using TRAP staining (Fig. 3C). In the TRAP-stained section, Tnfsf11$^{gum/+}$ mice exhibited a greater number and larger TRAP-positive osteoclasts compared to Tnfsf11$^{+/+}$ mice. To quantify this data, the ratio of TRAP-positive osteoclasts to trabecular bone surface (OCs/BS)

and the ratio of osteoclast number to bone area (OCs/mm^2) were assessed (Fig. 3D). These results confirmed that the OCs/BS% and OCs/mm^2 values in Tnfsf11$^{+/+}$ mice were significantly smaller than those of Tnfsf11$^{gum/+}$ mice.

In summary, Tnfsf11$^{gum/+}$ mice exhibited a decrease in CTX-1 and sRANKL levels, which are bone remodeling markers, leading to reduced osteoclast activity in bone sections. However, there was no corresponding change in the amount of OPG in serum, which is a counterpart to sRANKL.

mRNA Seq analysis of bone marrow cells in Tnfsf11$^{+/+}$ and Tnfsf11$^{gum/+}$ mice.

To investigate the gene expression levels associated with bone formation, massive mRNA sequencing. was conducted on bone marrow cells in Tnfsf11$^{+/+}$ and Tnfsf11$^{gum/+}$ mice. In the gene expression categories, 117 genes related to cell differentiation were significantly up-regulated in Tnfsf11$^{gum/+}$ mice, while 132 genes were down-regulated (Fig. 4A). Among them, genes with mRNA expression levels that increased by at least 2-fold were selected for further analysis (Fig. 4B). Only 38 genes were significantly up-regulated, and 15 genes were down-regulated by over 2-fold in Tnfsf11$^{gum/+}$ mice. The highest up-regulated gene, Gpx5, showed a 4.4-fold increase, while the lowest gene, Nubpl, exhibited a 0.413-fold decrease in expression in Tnfsf11$^{gum/+}$ mice, as depicted in the hierarchical clustering of gene expression in the heatmap.

Only a small number of mRNA expression levels, such as Gli1, Slc35b2, Lrrc17, and Junb in osteoblast-related gene categories, were significantly higher. Additionally, Tclirg1, Junb, Anxa2, and Atp6ap1 in osteoclast-related genes were

higher in Tnfsf11 $^{gum/+}$ mice (Fig. 4D). In addition, only 2 genes, Csf1r and Tclrg1, in the tooth eruption-related gene categories were significantly down-regulated and up-regulated in Tnfsf11$^{gum/+}$ mice compared with Tnfsf11$^{+/+}$ mice.

Taken together, the heterozygous mutant Tnfsf11$^{gum/+}$ mice showed very little genetic variation, especially a small number of genetic changes related to bone formation and tooth eruption were observed.

IV. DISCUSSION

The central role of TNFSF11, also known as RANKL, in the proliferation, differentiation, function, and survival of osteoclasts is well established [15]. The Tnfsf11 gene encodes a type II transmembrane protein that includes a membrane anchoring domain, a connecting stalk, and a receptor-binding ectodomain [16,17]. Both human and mouse RANKL are synthesized as glycoproteins consisting of 317 and 316 amino acids, respectively, and their structures are very similar [18,19]. Like all other TNF family cytokines investigated to date, the crystal structure of the extracellular domain responsible for biological activity of RANKL indicates that RANKL self-assembles into stable, non-covalently associated trimer [20]. In addition to being expressed at high levels in the skeletal and primary and secondary lymphoid tissues, RANKL expression can be detected in keratinocytes of the skin, mammary epithelial cells, heart, skeletal muscle, lung, stomach, placenta, thyroid, and brain [21,22]. RANKL also retains biological activity in a 31 kDa soluble form derived from proteolytic cleavage or alternative splicing [23]. RANKL is a key component of the RANK/RANKL/OPG signaling axis, which is a central motif in osteoclast differentiation [24]. Osteoblasts and stromal cells produce RANKL, which binds to the RANK receptor on osteoclast precursors and mature osteoclasts [4,25]. The presence of osteoclasts and bone resorption are both dependent on RANKL, as indicated by the absence of osteoclasts in RANKL mutant mice [26,27]. In our present study, Tnfsf11 heterozygous mutant mice, which are deficient in RANKL production for bone resorption, exhibited no TRAP-positive cells in femoral tissue.

In Tnfsf11 heterozygous mutant mice, there was no change in serum OPG levels, but the decrease in RANKL was more pronounced, leading to a decrease in the RANKL/OPG ratio. This decrease is considered to have resulted in a decrease in CTX-1 (C-telopeptide of collagen type 1), a marker of bone resorption. The OPG, a soluble decoy receptor for RANKL that inhibits osteoclast differentiation, is known to regulate osteoclast differentiation by maintaining a balance with RANKL. In this study, a reduction in RANKL levels in the body led to a significant decrease in bone resorption without any alteration in OPG levels. It is considered that the decreased RANKL did not lead to a decrease in OPG formation in osteoblasts in Tnfsf11 heterozygous mutant mice. In particular, the concentration of RANKL in the body is known to be closely related to tooth eruption and bone resorption [28,29]. Interestingly, in this study, tooth eruption proceeded normally in heterozygous Tnfsf11 mutant mice despite a decrease in RANKL concentration in the body. Considering the normal growth, survival rate, and typical tooth eruption of heterozygous Tnfsf11 mutant mice, only bone resorption is reduced as a result of decreased RANKL, and other aspects of growth and development are not significantly affected. For this reason, it is considered suitable as an experimental animal for studying bone resorption.

Genetic alterations associated with osteoblasts and osteoclasts also suggest that Tnfsf11 heterozygous mutant mice could serve as a viable experimental animal model for studying bone resorption, even in the absence of specific genetic mutations. Following a comprehensive mRNA sequencing analysis of bone marrow extracted cells, Tnfsf11 heterozygous mutant mice exhibited stable genetic profiles,

making them a reliable experimental animal model. Several upregulated mRNA expressions in genes related to osteoblasts or osteoclasts indicate that Tnfsf11 heterozygous mutant mice have reduced bone resorption activities solely due to decreased RANKL levels, without any genetic alterations. While the inversion identified in this model presented specific challenges to gene discovery, the phenotype is similar to other osteopetrotic models in that it exhibits reduced bone resorption in skeletal tissue [30,31]. However, we also identified a lack of fertility and failure of tooth eruption that has not been reported in other models. Other osteopetrotic mutants are anemic because their medullary cavity is completely solid, resulting in a lack of bone marrow.

While no viable candidate mutations were found using the standard exome pipeline, a strong candidate gene, Tnfsf11 (RANKL), was suggested due to its knockout phenotype, which includes osteopetrosis [32]. Manual read pair analysis of the alignment data using Integrated Genomics Viewer (IGV) revealed read mapping patterns consistent with an inversion. The data revealed an approximate 4.7 kb inversion involving exons 3 and 4, which was confirmed through PCR and Sanger sequencing across the inversion breakpoints.

V. CONCLUSION

In summary, the data demonstrate that a single gene mutation in Tnfsf11 leads to instability in bone resorption within the bone marrow cavity. This offers a unique approach to studying gene function in genetic contexts beyond a limited number of mouse strains. Furthermore, as a living collection that continues to identify and characterize mutants, this study provides a valuable resource for discovering genes related to bone biology.

REFERENCES

1. Kim NS, Kim HJ, Koo BK, et al. Receptor activator of NF-kappaB ligand regulates the proliferation of mammary epithelial cells via Id2. Mol Cell Biol. 2006;26:1002-13.

2. Boyce BF, Xing L. Biology of RANK, RANKL, and osteoprotegerin. Arthritis Res Ther. 2007;9 Suppl 1:S1.

3. Feng X. RANKing intracellular signaling in osteoclasts. IUBMB Life. 2005;57:389-95.

4. Ono T, Hayashi M, Sasaki F, Nakashima T. RANKL biology: bone metabolism, the immune system, and beyond. Inflamm Regen. 2020;40:2.

5. Darnay BG, Haridas V, Ni J, Moore PA, Aggarwal BB. Characterization of the intracellular domain of receptor activator of NF-kappaB (RANK). Interaction with tumor necrosis factor receptor-associated factors and activation of NF-kappab and c-Jun N-terminal kinase. J Biol Chem. 1998;273:20551-5.

6. Hikita A, Yana I, Wakeyama H, et al. Negative regulation of osteoclastogenesis by ectodomain shedding of receptor activator of NF-kappaB ligand. J Biol Chem. 2006;281:36846-55.

7. Park JH, Lee NK, Lee SY. Current Understanding of RANK Signaling in Osteoclast Differentiation and Maturation. Mol Cells. 2017;40:706-13.

8. Palmer K, Fairfield H, Borgeia S, et al. Discovery and characterization of spontaneous mouse models of craniofacial dysmorphology. Dev Biol. 2016;415:216-27.

9. Gritli-Linde A. The etiopathogenesis of cleft lip and cleft palate: usefulness and caveats of mouse models. Curr Top Dev Biol. 2008;84:37-138.

10. Murray SA. Mouse resources for craniofacial research. Genesis. 2011;49:190-9.

11. Li H, Yang Y, Hong W, Huang M, Wu M, Zhao X. Applications of genome editing technology in the targeted therapy of human diseases: mechanisms, advances and prospects. Signal Transduct Target Ther. 2020;5:1.

12. Kitsios GD, Zintzaras E. Genome-wide association studies: hypothesis-"free" or "engaged"? Transl Res. 2009;154:161-4.

13. McAlpine W, Russell J, Murray AR, Beutler B, Turer E. Research Techniques Made Simple: Forward Genetic Screening to Uncover Genes Involved in Skin Biology. J Invest Dermatol. 2019;139:1848-53 e1.

14. Davisson MT, Bergstrom DE, Reinholdt LG, Donahue LR. Discovery Genetics - The History and Future of Spontaneous Mutation Research. Curr Protoc Mouse Biol. 2012;2:103-18.

15. O'Brien CA. Control of RANKL gene expression. Bone. 2010;46:911-9.

16. Lang I, Fullsack S, Wyzgol A, et al. Binding Studies of TNF Receptor Superfamily (TNFRSF) Receptors on Intact Cells. J Biol Chem. 2016;291:5022-37.

17. Lang I, Fullsack S, Wyzgol A, et al. Correction: Binding studies of TNF receptor superfamily (TNFRSF) receptors on intact cells. J Biol Chem. 2020;295:11377.

18. Wright HL, McCarthy HS, Middleton J, Marshall MJ. RANK, RANKL and osteoprotegerin in bone biology and disease. Curr Rev Musculoskelet Med. 2009;2:56-64.

19. Liu C, Walter TS, Huang P, et al. Structural and functional insights of RANKL-RANK interaction and signaling. J Immunol. 2010;184:6910-9.

20. Ito S, Wakabayashi K, Ubukata O, Hayashi S, Okada F, Hata T. Crystal structure of the extracellular domain of mouse RANK ligand at 2.2-A resolution. J Biol Chem. 2002;277:6631-6.

21. Timotheadou E, Kalogeras KT, Koliou GA, et al. Evaluation of the Prognostic Value of RANK, OPG, and RANKL mRNA Expression in Early Breast Cancer Patients Treated with Anthracycline-Based Adjuvant Chemotherapy. Transl Oncol. 2017;10:589-98.

22. Taylor CR, Branstetter D, Manna E, Dougall WC, Bussiere J, Johnson CW. Distribution of RANK and RANK Ligand in Normal Human Tissues as Determined by an Optimized Immunohistochemical Method. Appl Immunohistochem Mol Morphol. 2017;25:299-307.

23. Buckle CH, De Leenheer E, Lawson MA, et al. Soluble rank ligand produced by myeloma cells causes generalised bone loss in multiple myeloma. PLoS One. 2012;7:e41127.

24. Infante M, Fabi A, Cognetti F, Gorini S, Caprio M, Fabbri A. RANKL/RANK/OPG system beyond bone remodeling: involvement in breast cancer and clinical perspectives. J Exp Clin Cancer Res. 2019;38:12.

25. Kim N, Kadono Y, Takami M, et al. Osteoclast differentiation independent of the TRANCE-RANK-TRAF6 axis. J Exp Med. 2005;202:589-95.

26. Suda T, Takahashi N, Udagawa N, Jimi E, Gillespie MT, Martin TJ. Modulation of osteoclast differentiation and function by the new members of the tumor

necrosis factor receptor and ligand families. Endocr Rev. 1999;20:345-57.

27. Xiong J, Cawley K, Piemontese M, et al. Soluble RANKL contributes to osteoclast formation in adult mice but not ovariectomy-induced bone loss. Nat Commun. 2018;9:2909.

28. Huang H, Wang J, Zhang Y, et al. Bone resorption deficiency affects tooth root development in RANKL mutant mice due to attenuated IGF-1 signaling in radicular odontoblasts. Bone. 2018;114:161-71.

29. Tanaka S, Nakamura K, Takahasi N, Suda T. Role of RANKL in physiological and pathological bone resorption and therapeutics targeting the RANKL-RANK signaling system. Immunol Rev. 2005;208:30-49.

30. Li H, Cheng X, Zhang L, et al. An Integration of Genome-Wide Association Study and Gene Co-expression Network Analysis Identifies Candidate Genes of Stem Lodging-Related Traits in Brassica napus. Front Plant Sci. 2018;9:796.

31. Bartolome N, Segarra S, Artieda M, et al. A genetic predictive model for canine hip dysplasia: integration of Genome Wide Association Study (GWAS) and candidate gene approaches. PLoS One. 2015;10:e0122558.

32. Meyts I, Bosch B, Bolze A, et al. Exome and genome sequencing for inborn errors of immunity. J Allergy Clin Immunol. 2016;138:957-69.

Fig. 1

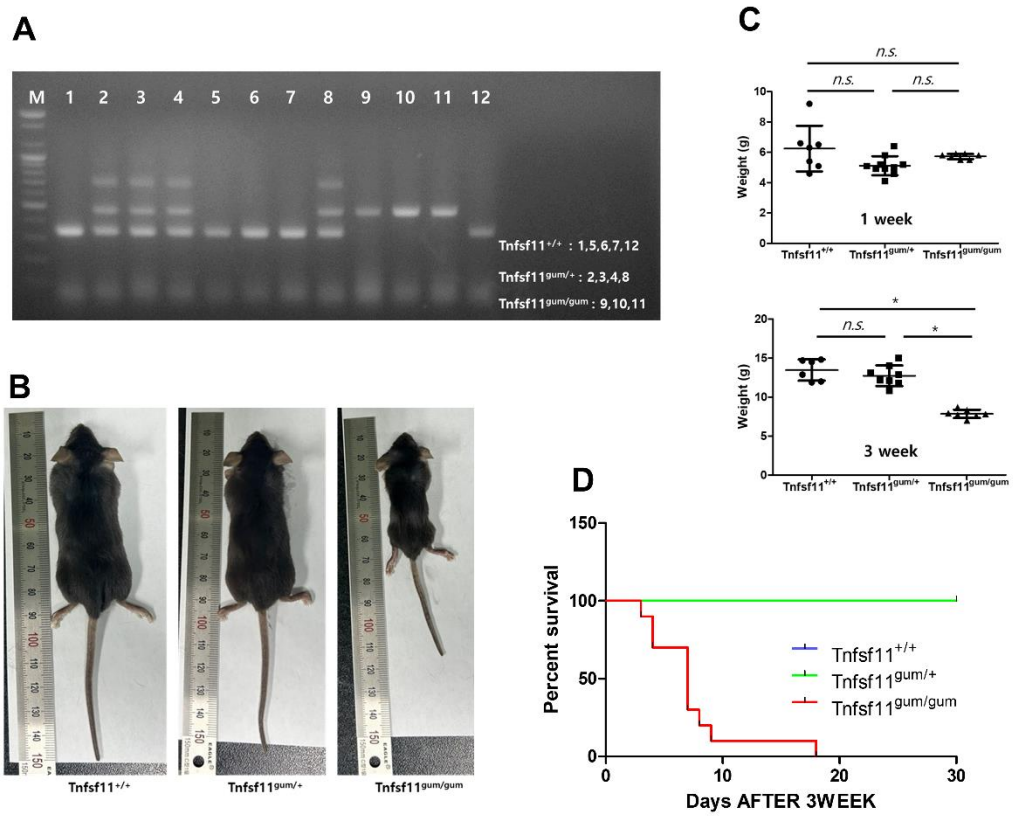

Figure 1. Charecterization of Tnfsf11$^{+/+}$, Tnfsf11$^{gum/+}$ and Tnfsf11$^{gum/gum}$ mice. A) The Tnfsf11$^{+/+}$, Tnfsf11$^{gum/+}$ and Tnfsf11$^{gum/gum}$ mice genotype and monitoring results. B) Size at 3 weeks and C) weight of Tnfsf11$^{+/+}$, Tnfsf11$^{gum/+}$ and Tnfsf11$^{gum/gum}$ mice. D) Survival rate after 3 weeks birth of Tnfsf11$^{+/+}$, Tnfsf11$^{gum/+}$ and Tnfsf11$^{gum/gum}$ mice. Results are representative of three separate experiments that had comparable results. Significance presents $*P<0.05$. *N.S.*, not significant.

Fig. 2

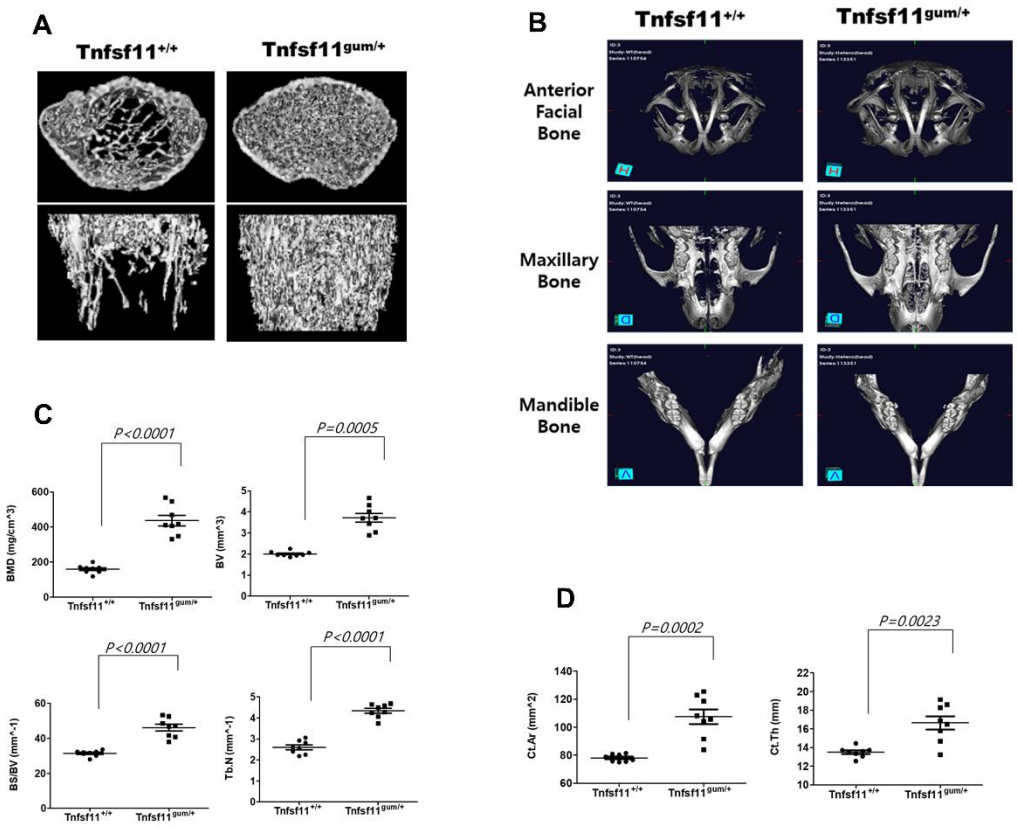

Figure. 2 Radiographic results of Tnfsf11$^{+/+}$ and Tnfsf11gum/+ mice. Micro CT image of 5 weeks Tnfsf11$^{+/+}$ and Tnfsf11$^{gum/+}$ A) mice femur and B) facial bone. Micro CT analysis of C) trabecular and D) cortical bone in Tnfsf11$^{+/+}$ and Tnfsf11$^{gum/+}$ mice femur. Results are representative of three separate experiments that had comparable results. Significance presents *P* value. *N.S.*, not significant.

Fig. 3

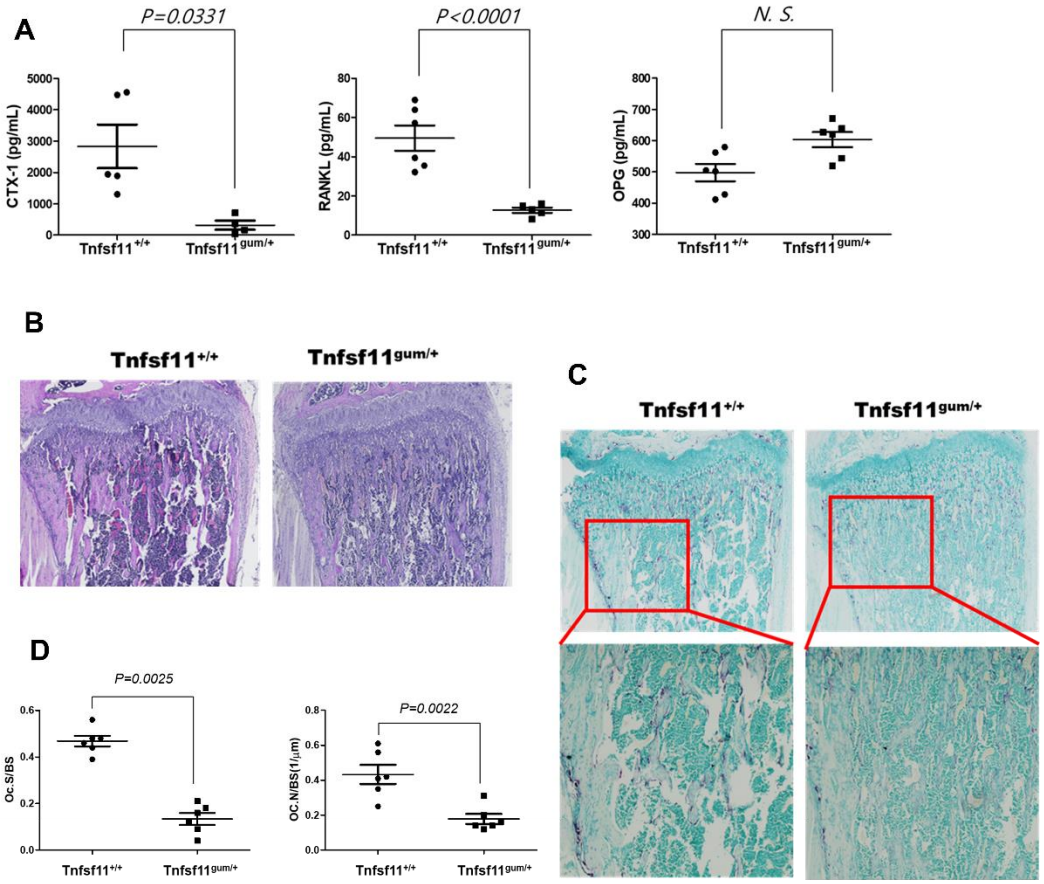

Figure. Bone resorption marker and histologic analysis in Tnfsf11$^{+/+}$ and Tnfsf11gum/+ mice. A) The CTX-1, RANKL and OPG level in Tnfsf11$^{+/+}$ and Tnfsf11$^{gum/+}$ mice serum. B) H&E staining and C) TRAP for histologic analysis in Tnfsf11$^{+/+}$ and Tnfsf11$^{gum/+}$ mice femur. D) Osteoclast surface/Bone Surface (Oc.S./B.S.) and Osteoclast number/Bone Surface (Oc.N./B.S.) were present. Results are representative of three separate experiments that had comparable results. Significance presents *P* value. *N.S.*, not significant.

Fig. 4

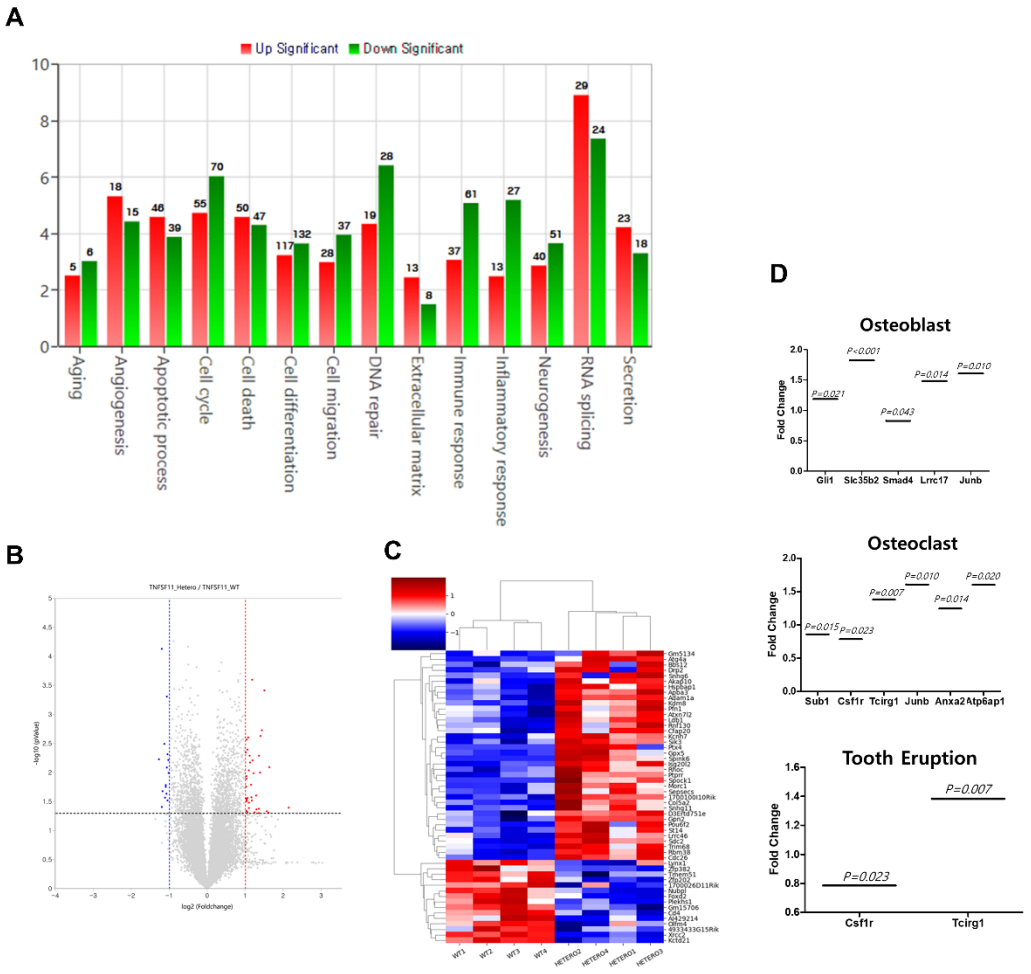

Figure. mRNA Seq analysis of bone marrow cells in Tnfsf11$^{+/+}$ and Tnfsf11$^{gum/+}$ mice femur. A) Categories of Total gene expression. B) Volcano analysis and C) Above 2 fold mRNA expressions of bone marrow cells in Tnfsf11$^{+/+}$ and Tnfsf11$^{gum/+}$ mice femur. Heatmap shows hierarchical clustering of gene expression. D) Osteoblast, Osteoclast and Tooth eruption related gene expression. Significance presents *P* value. *N.S.*, not significant.